

Easy-cone magnetic structure in $(\text{Cr}_{0.9}\text{B}_{0.1})\text{Te}$

Cite as: Appl. Phys. Lett. **116**, 102404 (2020); <https://doi.org/10.1063/5.0002118>

Submitted: 22 January 2020 . Accepted: 23 February 2020 . Published Online: 10 March 2020

Yangkun He, Gerhard H. Fecher , Johannes Kroder, Horst Borrmann, Xiao Wang, Lunyong Zhang, Chang-Yang Kuo, Cheng-En Liu, Chien-Te Chen, Kai Chen, Fadi Choueikani, Philippe Ohresser , Arata Tanaka, Zhiwei Hu, and Claudia Felser



View Online



Export Citation



CrossMark

ARTICLES YOU MAY BE INTERESTED IN

[Tunable positive magnetoresistance and crossover from weak antilocalization to weak localization transition in half-Heusler compounds \$\text{RPtBi}\$ \(\$\text{R}=\text{lanthanide}\$ \)](#)

Applied Physics Letters **116**, 101902 (2020); <https://doi.org/10.1063/1.5143990>

[Engineering skyrmions and emergent monopoles in topological spin crystals](#)

Applied Physics Letters **116**, 090501 (2020); <https://doi.org/10.1063/1.5139488>

[Synchronized excitation of magnetization dynamics via spin waves in Bi-YIG thin film by slot line waveguide](#)

Applied Physics Letters **116**, 102403 (2020); <https://doi.org/10.1063/1.5143519>

Lock-in Amplifiers
up to 600 MHz



Watch



Easy-cone magnetic structure in $(\text{Cr}_{0.9}\text{B}_{0.1})\text{Te}$

Cite as: Appl. Phys. Lett. **116**, 102404 (2020); doi: 10.1063/5.0002118

Submitted: 22 January 2020 · Accepted: 23 February 2020 ·

Published Online: 10 March 2020



View Online



Export Citation



CrossMark

Yangkun He,¹ Gerhard H. Fecher,^{1,a)}  Johannes Kroder,¹ Horst Borrmann,¹ Xiao Wang,¹ Lunyong Zhang,¹ Chang-Yang Kuo,^{1,2} Cheng-En Liu,^{1,2} Chien-Te Chen,³ Kai Chen,⁴ Fadi Choueikani,⁵ Philippe Ohresser,⁵  Arata Tanaka,⁶ Zhiwei Hu,¹ and Claudia Felser¹

AFFILIATIONS

¹Max Planck Institute for Chemical Physics of Solids, D-01187 Dresden, Germany

²Department of Electrophysics, National Chiao Tung University, Hsinchu 30010, Taiwan

³National Synchrotron Radiation Research Center, Hsinchu 30076, Taiwan

⁴Helmholtz Zentrum Berlin für Materialien und Energie, D-12489 Berlin, Germany

⁵Synchrotron SOLEIL, 91192 Gif-sur-Yvette, Cedex, France

⁶Department of Quantum Matter, ADSM, Hiroshima University, Higashi-Hiroshima 739-8526, Japan

^{a)} Author to whom correspondence should be addressed: fecher@cphys.mpg.de

ABSTRACT

Although stoichiometric CrTe is difficult to synthesize because of the appearance of Cr vacancies, ferromagnetic Cr_{1-x}Te compounds have attracted increasing attention. This work investigates single crystalline $(\text{Cr}_{0.9}\text{B}_{0.1})\text{Te}$ with the Cr vacancies filled by B to stabilize the hexagonal crystal structure and shift the Fermi energy. The structural and magnetic properties have been characterized by experimental measurements and *ab initio* calculations. A collinear spin structure with an easy axis along *c* is observed at high temperature, whereas the magnetic moments localized at the Cr atoms gradually tilt away from the *c*-axis below 140 K. A maximum tilt angle of 30° is observed at a temperature of 2 K.

© 2020 Author(s). All article content, except where otherwise noted, is licensed under a Creative Commons Attribution (CC BY) license (<http://creativecommons.org/licenses/by/4.0/>). <https://doi.org/10.1063/5.0002118>

Cr_{1-x}Te compounds have attracted increasing attention since the discovery of their ferromagnetism. Different crystalline and magnetic Cr_{1-x}Te phases have been reported for $0 < x < 0.4$. Different Cr contents *x* also result in a different Curie temperature (T_C) and saturation magnetization.¹ Cr_{1-x}Te has a hexagonal structure similar to binary CrTe, which has $T_C = 340$ K. However, although the Te layers are fully occupied in both cases, Cr_{1-x}Te has Cr vacancies in every second Cr layer. The Cr vacancies induce small deviations from the hexagonal symmetry, leading to monoclinic Cr_3Te_4 , trigonal Cr_2Te_3 , and trigonal and monoclinic Cr_5Te_8 .² In particular, Cr_5Te_8 is a strong uniaxial ferromagnet.^{3,4} However, at higher Cr concentrations, the magnetic structure is more complicated. For instance, a canted ferromagnetic structure was observed at low temperature by neutron diffraction^{5,6} and magnetization measurements.¹ Although the tendency to create vacancies makes the synthesis of stoichiometric CrTe difficult, the defects determine the magnetic moment of Cr and the magnetic structure of Cr_{1-x}Te , leading to a lower saturation magnetization and T_C .

The present work reports the magnetic and electronic properties of $(\text{Cr}_{0.9}\text{B}_{0.1})\text{Te}$ single crystals, where the Cr vacancies are filled by B, stabilizing the hexagonal structure as well as shifting the Fermi energy

and melting point. Measurements of the structural and magnetic properties are compared with *ab initio* calculations.

Single crystals of $(\text{Cr}_{0.9}\text{B}_{0.1})\text{Te}$ were grown by a step-by-step annealing process. Pure Cr (99.99%), Te (99.9999%), and B (99.999%) were ground into small pieces and mixed in an alumina tube. The alumina tube was sealed in a quartz tube filled with 20 kPa Ar. To reduce the evaporation of Te, the latter tube was heated gradually in the series: annealing to 873 K for 3 days, 1073 K for 1 day, and 1473 K for 5 days. Then, because a fast cooling is of vital importance, as a slow cooling would lead to the precipitation of Cr, the tube was cooled by immersion into ice water. The composition has been characterized by both energy-dispersive x-ray spectroscopy (EDS) and wavelength-dispersive x-ray spectroscopy (WDS). The samples have a homogeneous $\text{Cr}_{45.8}\text{B}_{3.4}\text{Te}_{50.9}$ composition that, using Te as the reference, corresponds to $\text{Cr}_{0.9}\text{B}_{0.07}\text{Te}_{1.0}$. This is in agreement with their nominal composition within the uncertainty of the methods used.

X-ray diffraction (XRD) and Laue patterns of the powder, taken at room temperature with Cu K_α radiation, are shown in Fig. 1. As seen, the hexagonal structure is confirmed. Binary CrTe crystallizes in the $B8_1$ structure (prototype: NiAs, hP4, $P6_3mmc$, 194)⁷ with Cr and

Te layers alternating. For $(\text{Cr}_{1-x}\text{B}_x)\text{Te}$ with $x \ll 1$, it is assumed that B replaces only Cr atoms of every second Cr layer. Consequently, Cr atoms are in two different environments: the Cr atoms in the unperturbed layer are labeled Cr^I and those in the layer with substituted B are labeled Cr^{II} . The resulting $\text{Cr}_{1-x}\text{B}_x$ ($x \ll 1$) structure belongs to space group $P\bar{3}m1$ (164), with Cr^I (97.3%) in Wyckoff position 1a (0,0,0) (in brackets, the site occupations from Rietveld refinement are given) and Te (98.6%) in 2d (2/3,1/3,1/4). Site 1b (0,0,1/2) is partially occupied by Cr^{II} (79.6%) and randomly distributed B (19.9%). The lattice constants $a = 4.0184 \text{ \AA}$ and $c = 6.2684 \text{ \AA}$ are in agreement with the values previously reported for similar compounds.^{1,7}

The electronic and magnetic structures were calculated from first principles in the local spin density approximation using the SPRKKR⁸ computer program in its full potential, fully relativistic mode. In this mode, instead of using a perturbational approach to the spin-orbit interaction, the spin-polarized Dirac equation with the 4-component Kohn-Sham wavefunction is solved. In particular, the generalized gradient approximation of Perdew *et al.*⁹ was used for the parametrization of the exchange-correlation functional. In the calculations for $(\text{Cr}_{0.9}\text{B}_{0.1})\text{Te}$, the random occupation of the 1b sites in the Cr-B layer was modeled through the coherent potential approximation implemented in SPRKKR. It should be noted that the calculations did not converge when B replaced Cr in both layers.

The fully relativistic electronic structure calculated is shown in Fig. 2. The smearing and broadening of the dispersion is a result of the chemical disorder scattering caused by the random distribution of Cr^{II} and B on site 1b. The density of states reveals the exchange splitting of the Cr 3d valence states. The density of the minority states exhibits a minimum at the Fermi energy (ϵ_F) resulting from a pseudogap.

Magnetization was measured using a vibrating sample magnetometer (MPMS 3, Quantum Design). The magnetic properties of $(\text{Cr}_{0.9}\text{B}_{0.1})\text{Te}$ single crystals are summarized in Fig. 3. The Curie temperature found is $T_C = 336 \text{ K}$. The magnetic moment at 2 K is $2.8 \mu_B$, which results in an average total magnetic moment per Cr atom of $m_{\text{Cr}} = 3.11 \mu_B$. The *ab initio* calculations result in spin (m_s) and orbital (m_l) magnetic moments per Cr atom, which are $m_s^I = 3.706 \mu_B$, $m_l^I = 0.007 \mu_B$ for Cr^I and $m_s^{II} = 3.717 \mu_B$, $m_l^{II} = 0.009 \mu_B$ for Cr^{II} . The overall magnetic moments in the four-site primitive cell are $m_s = 6.483 \mu_B$ and $m_l = -0.016 \mu_B$. The negative value of the overall orbital moment results from polarization of the Te atoms. However, as seen, the orbital moments are negligible. The magnetic

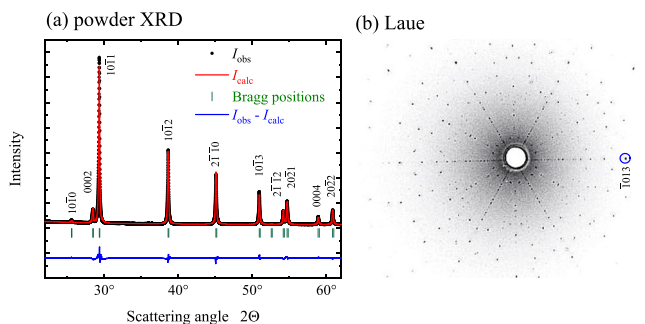


FIG. 1. Crystal structure of $(\text{Cr}_{0.9}\text{B}_{0.1})\text{Te}$. The very tiny 2020 reflexion of the powder XRD is not indexed. Only the 1013 reflexion is marked and indexed in the Laue pattern.

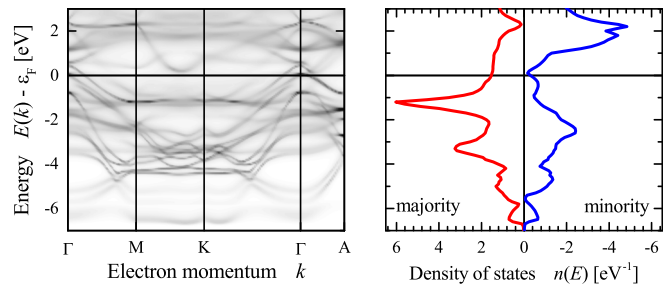


FIG. 2. Calculated electronic structure of $(\text{Cr}_{0.9}\text{B}_{0.1})\text{Te}$: (a) the Bloch spectral function, $E(k)$, and (b) the spin-resolved density of states, $n(E)$.

moments calculated for the Cr atoms are rather site-independent although they are higher than the average ones obtained experimentally.

The dependence of the magnetization along the c - and a -axes on the temperature is shown in Figs. 3(a) and 3(b), respectively, for different applied magnetic fields. At an applied field of 1 T, the saturation magnetization M_s increases to $90 \text{ Am}^2/\text{kg}$. At a low temperature and low field, a kink caused by spin reorientation appears, shifting in temperature with the size of the applied field. At a low magnetic field (0.01 T), the transition temperature T_{SR} is approximately 140 K, decreasing rapidly as the field along the c -axis increases, dropping to 118 K at 0.1 T. Conversely, it increases slightly to 142 K under a 0.45 T field along the a -axis. The spin reorientation is also observed in the AC susceptibility measurements of Fig. 3(c). Besides the Hopkinson effect¹⁰ observed near T_C , the AC susceptibility drastically decreases below 140 K to almost zero when the field is along the c -axis, while it slightly increases at temperatures below T_{SR} when the field is along the a -axis. The magnetization curves for both field directions at 300 and 2 K after correction of the demagnetizing factor are shown in Figs. 3(d) and 3(e), respectively. At 300 K, the magnetization of the crystal saturates at a small field along the c -axis, whereas a field of up to 0.44 T is required to saturate the sample along the a -axis. This is a typical easy-axis-type behavior. Therefore, the in-plane anisotropy can be assumed to be negligible. At 2 K, the magnetization along c saturates fast, similar to the 300 K case. However, at approximately 0.22 T along the a -axis, it displays a sudden curvature that does not exist in the linear curve of 300 K. This is because of the spin reorientation caused by the applied magnetic field. The coercivity along the c -axis at 2 K and 300 K is 0.011 T and lower than 0.003 T, respectively. Note that, below T_{SR} , the saturation magnetic field H_{sat} along the a -axis, i.e., the anisotropy field H_a , decreases gradually for decreasing temperature, different from normal easy-axis magnets. The magnetocrystalline anisotropy, calculated as explained in Ref. 11, is shown in Fig. 3(f). The anisotropy constant K_1 decreases from 240 kJm^{-3} at 200 K to -100 kJm^{-3} at 2 K, whereas K_2 increases from -40 kJm^{-3} at high temperature to 100 kJm^{-3} at 2 K. The negative K_1 and $K_2 > -K_1/2$ indicate an easy-cone-type structure with the cone angle given by $\sin(\theta) = \sqrt{-K_1/2K_2}$.^{11,12}

To determine the relation between the tilt angle and temperature, the magnetization of a single crystal is measured under a rotating magnetic field of 0.05 T, as shown in Fig. 3(g). Because the sample is cubic, it has a uniformly shaped anisotropy. Above T_{SR} , the angular dependence of the magnetization has a sinusoidal shape, with the largest value obtained along c . However, below T_{SR} , the curve gradually becomes asymmetric because of hysteresis, as shown from the

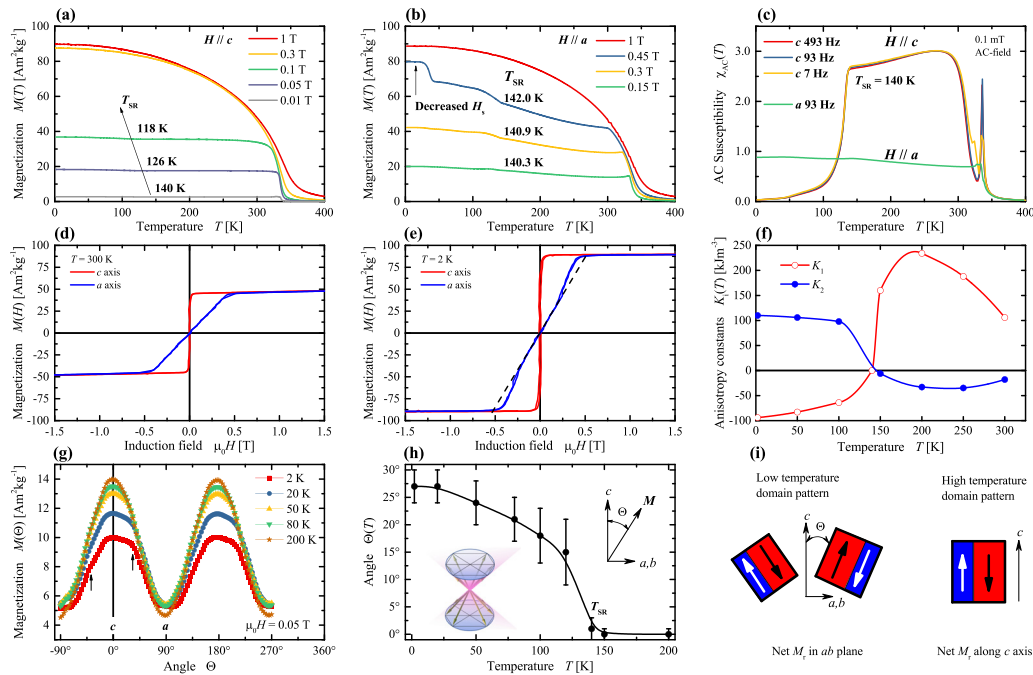


FIG. 3. Measured magnetic properties of $(\text{Cr}_{0.9}\text{B}_{0.1})\text{Te}$. (a) and (b) Temperature dependence of the magnetization at different applied magnetic fields along the (a) c -axis and (b) a -axis. The second step in the $M(T)$ curve of (b), marked by an arrow, does not correspond to a transition but rather resembles the decrease in the anisotropy field. (c) AC susceptibility, evidencing spin reorientation. (d) and (e) Hysteresis $M(H)$ loop at (d) 300 K and (e) 2 K. The black, dashed lines are linear fits of the initial magnetization. (f) Magnetocrystalline anisotropy at different temperatures. (g) Angular dependence of the magnetization (0.05 T), where 0° and 90° correspond to the c - and a -axes, respectively. (h) Temperature dependence of the tilt angle. (i) Schematics of the remanent magnetization below (left) and above (right) the spin reorientation transition.

evolution of the tilt angle with the temperature shown in Fig. 3(h). The tilt angle can be identified from the shoulders of the magnetization, which are indicated by arrows in Fig. 3(g). As seen, it decreases gradually from approximately 30° at 2 K to 0° at T_{SR} . The asymmetric shape of the magnetization curves is a result of non-equivalent directions. One is closer to the initial magnetization direction than the other. The angles obtained from the shoulders agree with those deduced from K_1 and K_2 . The value in Fig. 3(g) is smaller than that in Fig. 3(a) under 0.05 T, because of the cooling history. Figure 3(a) originates from a field cooling process, while the sample in Fig. 3(g) was cooled without the applied field and then magnetized initially along the a axis. The coercivity at low temperature is of the same order as the applied field (0.05 T) and influences the measured value too. Figure 3(i) illustrates the alignment of the magnetization in the remanent state. At high temperature, the spins as well as the remanence (M_r) are parallel to the c -axis. Below T_{SR} , the major component along the c -axis is compensated to reduce the stray field, whereas the minor component in the basal plane is not completely compensated, leading to a net M_r . When the field is lower than the coercivity—as is the case in the AC susceptibility measurements—the domain wall motion is forbidden; as a result, the AC susceptibility becomes zero. At moderate fields, instead, the behavior is that of an easy-axis magnet.

X-ray absorption spectra (XAS) were measured at the TPS45A beamline¹³ of the NSRRC synchrotron (Taiwan). The Cr $L_{2,3}$ XAS spectra measured at 300 K for $(\text{Cr}_{0.9}\text{B}_{0.1})\text{Te}$ and Cr_2O_3 , which were used as a reference, are shown in Fig. 4. The spectrum of $(\text{Cr}_{0.9}\text{B}_{0.1})\text{Te}$ is less structured and is shifted to lower energy by approximately

2–3 eV relative to Cr_2O_3 . This is attributed to the metallic nature of $(\text{Cr}_{0.9}\text{B}_{0.1})\text{Te}$ and to a change in the multiplet structure, i.e., to a different coupling of the $2p$ corehole with the $3d$ valence states of Cr. The energy shift can be understood by an increased covalence or a decrease in the charge transfer from oxygen to tellurium, which results in a gradual decrease in the charge transfer energy.

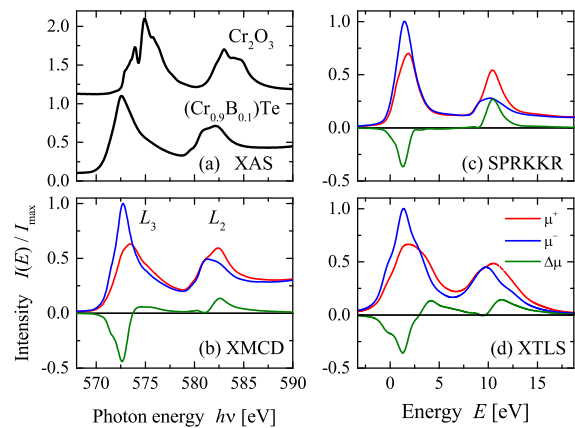


FIG. 4. X-ray absorption and magnetic circular dichroism. (a) XAS spectra of $(\text{Cr}_{0.9}\text{B}_{0.1})\text{Te}$ and Cr_2O_3 . (b) XMCD spectra measured for $(\text{Cr}_{0.9}\text{B}_{0.1})\text{Te}$. (c) and (d) Simulated Cr XMCD spectra obtained by (c) first principles and (d) atomic ligand-field multiplet calculations. (All intensities are normalized to the maxima at the L_3 edge.)

X-ray magnetic circular dichroism (XMCD) was measured to obtain a deeper understanding of the magnetic properties. The measurements were carried out at 10 K under a magnetic field of 6 T and at 100% circular polarization at the DEIMOS beamline of the SOLEIL synchrotron (France). Figure 4(b) shows the results of the measurements. For comparison, the results of the first principles calculations are reported in Fig. 4(c). The measured and calculated data are in agreement with a previous report on the Cr-Te system.¹⁴ As seen, the *ab initio* calculations reproduce the shape of the experimental spectra. The Cr 2*p* binding energies for the first Cr atom are calculated to be $E_{3/2}^I = -549.02$ eV and $E_{1/2}^I = -557.66$ eV and only 37 meV higher for the second Cr atom. For both atoms, the spin-orbit splitting is $\Delta_{SO} \approx 8.6$ eV, in agreement with the calculated value. The difference between the experimental and calculated spectra is caused by the secondary electron background in the measurements, which is not present in the calculations. However, further deviations may appear because of incomplete photon polarization or magnetization in the experiment.

To obtain the spin magnetic moment, the spin sum rule is commonly used.¹⁵ However, a strong overlap between the L_2 and L_3 edges leads to a large underestimation of the spin moment.^{16–18} Therefore, atomic ligand-field multiplet calculations were performed using the XTLS code.¹⁹ The CrTe₆ cluster parameters were set to $U_{dd} = 5.5$ eV, $U_{pd} = 7.0$ eV, $\Delta = 1.0$ eV, $10Dq = 1.0$ eV, $V(t_{2g}) = 1.56$ eV, $V(e_g) = 2.94$ eV, and $H_{ex} = 0.02$ eV along the z direction. The Slater integrals were scaled to 75% of the Hartree-Fock values. In the multiplet calculations, the charge transfer energy Δ needed to be reduced from 5.2 eV for Cr₂O₃²⁰ to 1.0 eV for (Cr_{0.9}B_{0.1})Te. This accounts for the increased covalence, corresponding to a lower charge transfer energy, when comparing Te with O. As shown in Fig. 4(d), the multiplet calculations, similar to the *ab initio* ones, reproduce the measured XMCD spectra of Fig. 4(b). The spin and orbital moments of Cr obtained from the multiplet calculation are 2.98 μ_B and 0.09 μ_B , respectively. This leads to a total moment of 3.07 μ_B , in good agreement with the measurements. Instead, the orbital moment obtained from XMCD is larger than the one obtained from the fully relativistic *ab initio* calculations by a factor 10.

In the current work, the structural and magnetic properties of synthesized (Cr_{0.9}B_{0.1})Te single crystals have been investigated. The structural, electronic, and magnetic measurements, including the XMCD ones, have been discussed and compared with *ab initio*

calculations. From our detailed magnetic investigations, it is concluded that (Cr_{0.9}B_{0.1})Te has a collinear spin structure with an easy axis along c at high temperature. Below 140 K, the magnetic moments localized at the Cr atoms gradually tilt away from the c -axis. The tilt angle is field- and temperature-dependent, having its maximum of 30° at 2 K.

This research was partially supported by ERC Advanced Grant (No. 742068) TOPMAT. Support from the Max Planck-POSTECH-Hsinchu Center for Complex Phase Materials is gratefully acknowledged.

REFERENCES

- ¹J. Dijkstra, H. H. Weitering, C. F. V. Bruggen, C. Haas, and R. A. de Groot, *J. Phys.: Condens. Matter* **46**, 9141 (1989).
- ²A. F. Andersen, *Acta Chem. Scand.* **24**, 3495 (1970).
- ³X. H. Luo, W. J. Ren, and Z. D. Zhang, *J. Magn. Mater.* **445**, 37 (2018).
- ⁴Y. Wang, J. Yan, J. Li, S. Wang, M. Song, J. Song, Z. Li, K. Chen, Y. Qin, L. Ling, H. Du, L. Cao, X. Luo, Y. Xiong, and Y. Sun, *Phys. Rev. B* **100**, 024434 (2019).
- ⁵T. Hirone and S. Chiba, *J. Phys. Soc. Jpn.* **15**, 1991 (1960).
- ⁶G. Street, E. Sawatzky, and K. Lee, *J. Phys. Chem. Solids* **34**, 1453 (1973).
- ⁷P. Villars and K. Cenzual, *Pearson's Crystal Data—Crystal Structure Database for Inorganic Compounds* (ASM International, Materials Park, Ohio, USA, 2012/13).
- ⁸H. Ebert, D. Koedderitzsch, and J. Minar, *Rep. Prog. Phys.* **74**, 096501 (2011).
- ⁹J. P. Perdew, K. Burke, and M. Ernzerhof, *Phys. Rev. Lett.* **77**, 3865 (1996).
- ¹⁰J. Hopkinson, *Philos. Trans. R. Soc. London, Ser. A* **180**, 443 (1889).
- ¹¹J. M. D. Coey, *Magnetism and Magnetic Materials* (Cambridge University Press, Cambridge, 2010).
- ¹²R. Skomski, H.-P. Oepen, and J. Kirschner, *Phys. Rev. B* **58**, 11138 (1998).
- ¹³H.-M. Tsai, H.-W. Fu, C.-Y. Kuo, L.-J. Huang, C.-S. Lee, C.-Y. Hua, K.-Y. Kao, H.-J. Lin, H.-S. Fung, S.-C. Chung, C.-F. Chang, A. Chainani, L. H. Tjeng, and C.-T. Chen, *AIP Conf. Proc.* **2054**, 060047 (2019).
- ¹⁴K. Yaji, A. Kimura, C. Hirai, M. Taniguchi, M. Koyama, H. Sato, K. Shimada, A. Tanaka, T. Muro, S. Imada, and S. Suga, *Phys. Rev. B* **70**, 064402 (2004).
- ¹⁵P. Carra, B. T. Thole, M. Altarelli, and X. Wang, *Phys. Rev. Lett.* **70**, 694 (1993).
- ¹⁶Y. Teramura, A. Tanaka, and T. Jo, *J. Phys. Soc. Jpn.* **65**, 1053 (1996).
- ¹⁷G. van der Laan, K. T. Moore, J. G. Tobin, B. W. Chung, M. A. Wall, and A. J. Schwartz, *Phys. Rev. Lett.* **93**, 09740 (2004).
- ¹⁸C. Piamonteze, P. Miedema, and F. M. F. de Groot, *Phys. Rev. B* **80**, 184410 (2009).
- ¹⁹A. Tanaka and T. Jo, *J. Phys. Soc. Jpn.* **63**, 2788 (1994).
- ²⁰A. E. Bocquet, T. Mizokawa, K. Morikawa, A. Fujimori, S. R. Barman, K. Maiti, D. D. Sarma, T. Tokura, and M. Onoda, *Phys. Rev. B* **53**, 1161 (1996).